Publication Year	2018
Acceptance in OA@INAF	2021-02-10T14:06:56Z
Title	Exploring cosmic origins with CORE: The instrument
Authors	de Bernardis, P.; Ade, P. A. R.; Baselmans, J. J. A.; Battistelli, E. S.; Benoit, A.; et al.
DOI	10.1088/1475-7516/2018/04/015
Handle	http://hdl.handle.net/20.500.12386/30286
Journal	JOURNAL OF COSMOLOGY AND ASTROPARTICLE PHYSICS
Number	2018

Prepared for submission to JCAP

Exploring Cosmic Origins with CORE: The Instrument

P. de Bernardis, [1;2;a] P. A. R. Ade, [3] J.J.A. Baselmans, [4] E. S. Battistelli, [1;2] A. Benoit, [5] M. Bersanelli, [6;7] A. Bideaud, [5] M. Calvo, [5] F. J. Casas, [8] G. Castellano, [9] A. Catalano, [10] I. Charles, [11] I. Colantoni, [9] F. Columbro [1;2] A. Coppolecchia, [1;2] M. Crook, [12] G. D'Alessandro, [1;2] M. De Petris, [1;2] J. Delabrouille, [13] S. Doyle, [14] C. Franceschet, [6] A. Gomez, [15] J. Goupy, [5] S. Hanany, [16] M. Hills, [17] L. Lamagna, [1;2] J. Macias-Perez, [10] B. Ma ei, [18] S. Martin, [11] E. Martinez-Gonzalez, [8] S. Masi, [1;2] D. McCarthy, [19] A. Mennella, [6] A. Monfardini, [5] F. Noviello, [3] A. Paiella, [1;2] F. Piacentini, [1;2] M. Piat, [13] G. Pisano, [3] G. Signorelli, [20] C. Y. Tan, [16] A. Tartari, [13] N. Trappe, [19] S. Triqueneaux, [5] C. Tucker, [3] G. Vermeulen, [5] K. Young, [16] M. Zannoni, [21;22] A. Achœcarro, [23;24] R. Allison, [25] M. Ashdown, [26;27] M. Ballardini, [28;29;30] A. J. Banday, [31] R. Banerji, [13] J. Bartlett, [13] N. Bartolo, [28;32;33] S. Basak, [34;35] A. Bonaldi, [36] M. Bonato, [37;35] J. Borrill, [38] F. Bouchet, [39] F. Boulanger, [18] T. Brinckmann, [40] M. Bucher, [13] C. Burigana, [29;42;30] A. Buzzelli, [1;42;43] Z. Y. Cai, [44] C. S. Carvalho, [45] A. Challinor, [46] J. Chluba, [47] S. Clesse, [40] G. De Gasperis, [42;43] G. De Zotti, [48] E. Di Valentino, [39;49] J. M. Diego, [8] J. Errard, [50] S. Feeney, [26;51] R. Fernandez-Cobos, [8] F. Finelli, [29;30] F. Forastieri, [52] S. Galli, [39] R. GØnova-Santos, [53;54] M. Gerbino, [55] J. GonzÆlez-Nuevo, [56] S. Hagstotz, [57;58] J. Greenslade, [26] W. Handley, [26;27] C. HernÆndez-Monteagudo, [59] C. Hervias-Caimapo, [47] E. Hivon, [39] K. Kiiveri, [60;61] T. Kisner, [62] T. Kitching, [63] M. Kunz, [64] H. Kurki-Suonio, [60;61] A. Lasenby, [26;27] M. Lattanzi, [52] J. Lesgourgues, [40] A. Lewis, [65] M. Liguori, [28;32;48] V. Lindholm, [60;61] G. Luzzi, [1] C. J. A. P. Martins, [64] A. Melchiorri, [1;2] J. B. Melin, [10] D. Molinari, [41;52;29] P. Natoli, [41;52] M. Negrello, [3] A. Notari, [65] D. Paoletti, [29;30] G. Patanchon, [13] L. Polastri, [41;52] G. Polenta, [66;67] A. Pollo, [68] V. Poulin, [69;40] M. Quartin, [70;71] M. Remazeilles, [47] M. Roman, [72] J. A. Rubiæo-Martín, [53;54] L.

[a] Corresponding author

arXiv:1705.02170v2 [astro-ph.IM] 22 May 2017

Salvati, [1;2] M. Tomasi, [6;7] D. Tramonte, [53] T. Trombetti, [29;42;30] J. Väliviita, [60;61] R. Van de Weijgaert, [4;59] B. van Tent, [73] V. Vennin, [74] P. Vielva, [8] N. Vittorio, [42;43] for the CORE collaboration

[1]Dipartimento di Fisica, UniversitÆ di Roma La Sapienza , P.le A. Moro 2, 00185 Roma, Italy

[2]INFN, Sezione di Roma, P.le A. Moro 2, 00185 Roma, Italy

[3]School of Physics and Astronomy, Cardi University, The Parade, Cardi CF24 3AA, UK

[4]SRON - Netherlands Institute for Space Research, Sorbonnelaan 2, 3584 CA - Utrecht, The Netherlands

[5]Institut NØel, CNRS and UniversitØ Grenoble Alpes, F-38042 Grenoble, France

[6]Dipartimento di Fisica, UniversitÆ degli Studi di Milano, Via Celoria 16, I-20133 Milano, Italy

[7]INAF IASF, Via Bassini 15, I-20133 Milano, Italy

[8]Instituto de Fisica de Cantabria (CSIC-UC), Avda. los Castros s/n, 39005 Santander, Spain

[9]Istituto di Fotonica e Nanotecnologie - CNR, Via Cineto Romano 42, I-00156 Roma, Italy

[10]Laboratoire de Physique Subatomique & Cosmologie IN2P3 (CNRS), UniversitØ Grenoble Alpes, Grenoble, FR

[11]Univ. Grenoble Alpes, CEA INAC-SBT, 38000 Grenoble, France

[12]STFC - RAL Space - Rutherford Appleton Laboratory, OX11 0QX Harwell Oxford, UK

[13]APC, AstroParticule et Cosmologie, UniversitØ Paris Diderot, CNRS/IN2P3, CEA/lrfu, Observatoire de Paris, Sorbonne Paris CitØ, 10, rue Alice Domon et LØonie Duquet, 75205 Paris Cedex 13, France

[14]School of Physics and Astronomy, Cardi University, The Parade, Cardi CF24 3AA, UK

[15]Centro de Astrobiología (INTA-CSIC), Ctra. Torrejon-Ajalvir km. 4, 28850 Torrejon de Ardoz, Spain

[16]School of Physics and Astronomy and Minnesota Institute for Astrophysics, University of Minnesota/Twin Cities, USA

[17]STFC - RAL Space - Rutherford Appleton Laboratory, OX11 0QX Harwell Oxford, UK

[18]Institut d'Astrophysique Spatiale, CNRS, UMR 8617, UniversitØ Paris-Sud 11, Bâtiment 121, 91405 Orsay, France

[19]Department of Experimental Physics, Maynooth University, Maynooth, Co. Kildare, W23 F2H6, Ireland

[20]INFN, Sezione di Pisa, Largo Bruno Pontecorvo 2, 56127 Pisa, Italy

[21]Dipartimento di Fisica, UniversitÆ di Milano Bicocca, Milano, Italy

[22]INFN, sezione di Milano Bicocca, Milano, Italy

[23]Instituut-Lorentz for Theoretical Physics, Universiteit Leiden, 2333 CA, Leiden, The Netherlands

[24]Department of Theoretical Physics, University of the Basque Country UPV/EHU, 48040 Bilbao, Spain

[25]Institute of Astronomy, Madingley Road, Cambridge, CB3 0HA, UK

[26]Astrophysics Group, Cavendish Laboratory, Cambridge, CB3 0HE, UK

[27]Kavli Institute for Cosmology, Madingley Road, Cambridge, CB3 0HA, UK

[28]DIFA, Dipartimento di Fisica e Astronomia, UniversitÆ di Bologna, Viale Berti Pichat, 6/2, I-40127 Bologna, Italy

[29]INAF/IASF Bologna, via Gobetti 101, I-40129 Bologna, Italy
[30]INFN, Sezione di Bologna, Via Irnerio 46, I-40127 Bologna, Italy
[31]UniversitØ de Toulouse, UPS-OMP, IRAP, F-31028 Toulouse cedex 4, France, and CNRS, IRAP, 9 Av. colonel Roche, BP 44346, F-31028 Toulouse cedex 4, France
[32]INFN, Sezione di Padova, Via Marzolo 8, I-35131 Padova, Italy
[33]INAF-Osservatorio Astronomico di Padova, Vicolo dell Osservatorio 5, I-35122 Padova, Italy
[34]Department of Physics, Amrita School of Arts & Sciences, Amritapuri, Amrita Vishwa Vidyapeetham, Amrita University, Kerala 690525 India
[35]SISSA, Via Bonomea 265, 34136, Trieste, Italy
[36]Jodrell Bank Centre for Astrophysics, School of Physics and Astronomy, The University of Manchester, Oxford Road, Manchester M13 9PL, UK
[37]Department of Physics & Astronomy, Tufts University, 574 Boston Avenue, Medford, MA, USA
[38]Computational Cosmology Center, Lawrence Berkeley National Laboratory, Berkeley, California, U.S.A.
[39]Institut d' Astrophysique de Paris (UMR7095: CNRS & UPMC-Sorbonne Universities), F-75014, Paris, France
[40]Institute for Theoretical Particle Physics and Cosmology (TTK), RWTH Aachen University, D-52056 Aachen, Germany.
[41]Dipartimento di Fisica e Scienze della Terra, UniversitÆ di Ferrara, Via Giuseppe Saragat 1, I-44122 Ferrara, Italy
[42]Dipartimento di Fisica, UniversitÆ di Roma Tor Vergata, Via della Ricerca Scienti ca 1, I-00133, Roma, Italy
[43]INFN, Sezione di Roma 2, Via della Ricerca Scienti ca 1, I-00133, Roma, Italy
[44]CAS Key Laboratory for Research in Galaxies and Cosmology, Department of Astronomy, University of Science and Technology of China, Hefei, Anhui 230026, China
[45]Institute of Astrophysics and Space Sciences, University of Lisbon, Tapada da Ajuda, 1349-018 Lisbon, Portugal
[46]DAMTP, Centre for Mathematical Sciences, Wilberforce road, Cambridge, CB3 0WA, UK
[47]Jodrell Bank Centre for Astrophysics, School of Physics and Astronomy, The University of Manchester, Oxford Road, Manchester M13 9PL, UK
[48]INAF-Osservatorio Astronomico di Padova, Vicolo dell Osservatorio 5, I-35122 Padova, Italy
[49]Sorbonne UniversitØs, Institut Lagrange de Paris (ILP), F-75014, Paris, France
[50]Institut Lagrange, LPNHE, place Jussieu 4, 75005 Paris, France.
[51]Center for Computational Astrophysics, 160 5th Avenue, New York, NY 10010, USA
[52]INFN, Sezione di Ferrara, Via Saragat 1, 44122 Ferrara, Italy
[53]Instituto de Astrofísica de Canarias, C/Vía LÆctea s/n, La Laguna, Tenerife, Spain
[54]Departamento de Astrofísica, Universidad de La Laguna (ULL), La Laguna, Tenerife, 38206 Spain
[55]The Oskar Klein Centre for Cosmoparticle Physics, Department of Physics, Stockholm University, AlbaNova, SE-106 91 Stockholm, Sweden
[56]Departamento de Física, Universidad de Oviedo, C. Calvo Sotelo s/n, 33007 Oviedo, Spain
[57]Centro de Estudios de Física del Cosmos de Aragón (CEFCA), Plaza San Juan, 1, planta 2, E-44001, Teruel, Spain

[58]Faculty of Physics, Ludwig-Maximilians Universität, Scheinerstrasse 1, D-81679 Munich, Germany
[59]Excellence Cluster Universe, Boltzmannstr. 2, D-85748 Garching, Germany
[60]Department of Physics, Gustaf Hällströmin katu 2a, University of Helsinki, Helsinki, Finland
[61]Helsinki Institute of Physics, Gustaf Hällströmin katu 2, University of Helsinki, Helsinki, Finland
[62]Computational Cosmology Center, Lawrence Berkeley National Laboratory, Berkeley, California, U.S.A.
[63]Mullard Space Science Laboratory, University College London, Holmbury St Mary, Dorking, Surrey RH5 6NT, UK
[64]DØpartement de Physique ThØorique and Center for Astroparticle Physics, UniversitØ de GenŁve, 24 quai Ansermet, CH 1211 GenŁve 4, Switzerland
[65]Department of Physics & Astronomy, University of Sussex, Brighton BN1 9QH, UK
[66]Agenzia Spaziale Italiana Science Data Center, Via del Politecnico snc, 00133, Roma, Italy
[67]INAF - Osservatorio Astronomico di Roma, via di Frascati 33, Monte Porzio Catone, Italy
[68]National Center for Nuclear Research, ul. Ho»a 69, 00-681 Warsaw, Poland, and The Astronomical Observatory of the Jagiellonian University, ul. Orla 171, 30-244 Kraków, Poland
[69]LAPTh, UniversitØ Savoie Mont Blanc & CNRS, BP 110, F-74941 Annecy-le-Vieux Cedex, France
[70]Instituto de Fí sica, Universidade Federal do Rio de Janeiro, 21941-972, Rio de Janeiro, Brazil
[71]Observatório do Valongo, Universidade Federal do Rio de Janeiro, Ladeira Pedro Antônio 43, 20080-090, Rio de Janeiro, Brazil
[72]Laboratoire de Physique NuclØaire et des Hautes Énergies (LPNHE), UniversitØ Pierre et Marie Curie, Paris, France
[73]Laboratoire de Physique ThØorique (UMR 8627), CNRS, UniversitØ Paris-Sud, UniversitØ Paris Saclay, Bâtiment 210, 91405 Orsay Cedex, France
[74]Institute of Cosmology and Gravitation, University of Portsmouth, Dennis Sciama Building, Burnaby Road, Portsmouth PO1 3FX, United Kingdom

E-mail: paolo.debernardis@roma1.infn.it

Abstract. We describe a space-borne, multi-band, multi-beam polarimeter aiming at a precise and accurate measurement of the polarization of the Cosmic Microwave Background. The instrument is optimized to be compatible with the strict budget requirements of a medium-size space mission within the Cosmic Vision Programme of the European Space Agency. The instrument has no moving parts, and uses arrays of diffraction-limited Kinetic Inductance Detectors to cover the frequency range from 60 GHz to 600 GHz in 19 wide bands, in the focal plane of a 1.2 m aperture telescope cooled at 140 K, allowing for an accurate extraction of the CMB signal from polarized foreground emission. The projected CMB polarization survey sensitivity of this instrument, after foregrounds removal, is 1.7 μK arcmin. The design is robust enough to allow, if needed, a downscoped version of the instrument covering the 100 GHz to 600 GHz range with a 0.8 m aperture telescope cooled at 85 K, with a projected CMB polarization survey sensitivity of 3.2 μK arcmin.

Contents

1 Introduction 2

2 Telescope 5
2.1 Gregorian Design 6
2.1.1 All Re ective Design 6
2.1.2 Re ective/Refractive Design 7
2.2 Crossed Dragone 9
2.3 Telescope Summary 12

3 Polarization Modulator 12

4 Focal Plane 13
4.1 Mission Constraints 13
4.2 Radiation Coupling 14

5 Detectors 17
5.1 Detection Technology 18
5.2 Low Frequencies (channels: 60 GHz - 115 GHz): 18
5.3 CMB Frequencies (channels: 130 GHz - 220 GHz): 20
5.4 High Frequencies (channels: 255 GHz - 600 GHz): 21
5.5 KID Susceptibility to Cosmic Rays 23
5.6 Readout Electronics 24

6 Cryogenic System 24
6.1 Coolers 28
6.2 Closed Cycle Dilution Refrigerator 28
6.3 Focal Plane Suspension with Thermal Intercepts 30
6.4 1:7 K ^{3}He Joule-Thompson expansion cooler requirements 33

7 Instrument Calibration 34
7.1 Ground Calibration 35
7.2 In- ight calibration 36

8 Downscoping Options 36

9 Conclusions 38

10 Acknowledgements 38

1 Introduction

The measurement of the polarization state of the CMB promises to shed light on the earliest phases of the evolution of the Universe, testing the cosmic in ation scenario, but poses di cult experimental challenges, requiring a polarimeter with very high sensitivity, exquisite control of systematic e ects, and the ability to extract the tiny in ation-related signal from overwhelming polarized foregrounds.

In this paper we describe a space-based instrument, optimized to represent the ultimate experiment for probing cosmic in ation measuring CMB polarization (an objective which cannot be achieved by ground-based experiments alone, nor by simpler space-missions), while ful lling the stringent requirements of a medium-class mission of the European Space Agency. We underline that also the lack of detection of primordial B-modes by CORE would have an impact on the current cosmological paradigm, since a large part of in ation scenarios would be ruled out.

This paper is part of a series describing the CORE (Cosmic ORigins Explorer) mission and its scienti c context. Here we aim at an instrument baseline description with a level of detail adequate for starting a Phase-A study.

The CORE instrument inherits the legacy of Planck, as well as our previous proposals COrE and COrE+.

The goal of CORE is to detect unambiguously a tensor to scalar ratior as small as $1 \quad 10^{3}$ (3 CL), even in the presence of complex polarized foregrounds. In fact, the Starobinsky model, R^2 (Higgs) in ation, foresees $r > 2 \quad 10^{3}$. With this level of sensitivity, a null result would basically disfavour most of the large- eld in ation models allowed by Planck (see the companion paper on in ation [1]).

This ultimate measurement is possible only from space and requires a mission that will map the CMB B-modes polarization over most of the sky, with an angular resolution of a few arcminutes and with a polarization survey sensitivity better than 2:5 µK per square arcminute pixel, after foreground removal (20 times better than the aggregated CMB polarization sensitivity of the entire set of Planck polarized detectors). This mission will collect virtually all the information about the Early Universe encoded in the CMB polarization.

The CORE instrument builds on the success of Planck and Herschel, re-using many of the subsystems and methods developed by the mm/submm community. The sensitivity requirements described above, combined with the requirement of internal control of polarized foregrounds, drives the dimension of the focal plane of the instrument. The proposed CORE baseline instrument is based on an array of 2100 cryogenically cooled, linearly polarized detectors at the focus of a 1.2 meter aperture telescope. The entire sky will be surveyed with 19 frequency bands, spanning the range 60 to 600 GHz. The spacecraft will be located in a large Lissajous orbit around the Sun-Earth L2 Lagrange point to keep the Sun, Earth and Moon well away from the line of sight at all times, and thus avoid that they pollute the scienti c signal with unwanted far sidelobe contamination. The combination of three rotations of the spacecraft at di erent timescales provides an observation pattern such that each sky pixel is crossed frequently, and from many di erent directions. This scan strategy provides for a strong mitigation of systematic e ects and would thus ensure optimal use of the high inherent sensitivity, especially for extracting the large angular scale signals.

With this implementation, CORE also addresses a broad range of other questions of prime scienti c importance that cannot be answered by any other means than very accurate observation of the CMB polarization on all angular scales and over the near full sky. It

will probe the distribution of clustered mass in the Universe through the observation of the lensing of CMB polarization due to dark matter structures between our telescopes and the last scattering surface. The reconstruction of the CMB lensing potential will provide high signal-to-noise-ratio maps of the distribution of dark matter at redshifts $z = 1 - 3$ without recourse to biased baryonic tracers. In addition to providing a map of the dark matter integrated along the line of sight up to high redshift, this measurement, combined with cosmological constraints from Euclid, will constrain the sum of the 3 light neutrino masses with a statistical error of 3 meV, 5 times better than any single cosmological probe alone and su cient to distinguish unambiguously between a normal neutrino hierarchy ($m_1; m_2 \ll m_3$) with a mass sum of approximately at least 60 meV, and an inverted hierarchy ($m_3 \ll m_1; m_2$) with a minimal mass sum of about 100 meV (see the companion paper on cosmological parameters [2]).

CORE will also probe the distribution of hot gas up to redshifts $z = 2 - 3$ by measuring the thermal Sunyaev-Zel'dovich e ect, the inverse Compton scattering of CMB photons by energetic electrons. It will detect $\sim 50{,}000$ galaxy clusters extending to high redshift, more than 300000 clusters in combination with high-resolution ground-based surveys, and part of the hot baryons in the cosmic web. Combined with high resolution (2-3$'$) ground-based CMB data in atmospheric windows between 90 and 250 GHz, CORE will also detect the individual peculiar motions of $\sim 30{,}000$ galaxy clusters, thus directly measuring the cosmic velocity eld at large redshift, a measurement that cannot be performed by any other means (see the companion paper on clusters science [3]).

At frequencies above 350 GHz, where sky signals are dominated by emission from thermal dust and point sources, CORE will for the rst time provide full sky, high quality polarization maps. These maps will provide astrophysicists with the most detailed view yet at the Galactic magnetic eld, unveiling its role in creating the lamentary, web-like, structures where stars form. Magneto-hydrodynamical turbulence will be revealed with unprecedented statistical information characterizing the energy injection and energy transfer down to dissipation scales. The spectral dependence of the polarized signal from dust will be measured with high accuracy across the sky, furthering our understanding of the nature of interstellar dust. Moreover, together with the corresponding high sensitivity intensity maps, these observations will discover and characterize a large number of new galactic and extragalactic point sources and also measure their polarization properties.

Achieving the CORE cosmological science programme will require accurate separation of the many astrophysical foregrounds as well as exquisite control and assessment of systematic errors. The CORE instrument con guration and calibration procedure are designed to generate all the data needed for this assessment. In particular, the CORE array will include a large number of closely packed spectral bands for optimal monitornig of polarized foreground components. Simulations based on the full presently available information, as summarized in the Planck Sky Model [4], and analyzed using state-of-the-art component separation algorithms show that CORE will achieve its science objectives and that the design includes redundancy and margin for error. This is described in detail in the mission paper of this series [5].

The CORE ultra-high sensitivity maps of the three Stokes parameters I, Q, and U in 19 frequency bands will serve as a long standing legacy and a reference dataset for the microwave and submillimeter emission in both intensity and polarization over the full sky. Astrophysicists will mine these maps for decades. In addition to the compelling science deliverables we know about today, even more exciting are all the discoveries buried in these maps, and that we can not yet imagine, nor describe.

Other missions with similar targets have been proposed in the past. Apart from our

channel GHz	beam arcmin	N_{det}	T μK arcmin	P μK arcmin	I μK_{RJ} arcmin	I kJy=sr arcmin	y 10^6 y_{SZ} arcmin	PS (5) mJy
60	17.87	48	7.5	10.6	6.81	0.75	-1.5	5.0
70	15.39	48	7.1	10	6.23	0.94	-1.5	5.4
80	13.52	48	6.8	9.6	5.76	1.13	-1.5	5.7
90	12.08	78	5.1	7.3	4.19	1.04	-1.2	4.7
100	10.92	78	5.0	7.1	3.90	1.2	-1.2	4.9
115	9.56	76	5.0	7.0	3.58	1.45	-1.3	5.2
130	8.51	124	3.9	5.5	2.55	1.32	-1.2	4.2
145	7.68	144	3.6	5.1	2.16	1.39	-1.3	4.0
160	7.01	144	3.7	5.2	1.98	1.55	-1.6	4.1
175	6.45	160	3.6	5.1	1.72	1.62	-2.1	3.9
195	5.84	192	3.5	4.9	1.41	1.65	-3.8	3.6
220	5.23	192	3.8	5.4	1.24	1.85	-	3.6
255	4.57	128	5.6	7.9	1.30	2.59	3.5	4.4
295	3.99	128	7.4	10.5	1.12	3.01	2.2	4.5
340	3.49	128	11.1	15.7	1.01	3.57	2.0	4.7
390	3.06	96	22.0	31.1	1.08	5.05	2.8	5.8
450	2.65	96	45.9	64.9	1.04	6.48	4.3	6.5
520	2.29	96	116.6	164.8	1.03	8.56	8.3	7.4
600	1.98	96	358.3	506.7	1.03	11.4	20.0	8.5
Array		2100	1.2	1.7			0.41	

Table 1 : ProposedCORE frequency channels. The baseline aperture of the telescope is 1.2m in diameter. The detectors are cooled at 0.1K and their sensitivity is calculated assuming = = 30% bandwidth, 60% optical e ciency, total noise of twice the expected photon noise from the sky and the optics of the instrument at 40 K. This con guration has 2100 detectors, about 45% of which are located in CMB channels between 130 and 220 GHz. Those six CMB channels yield an aggregated CMB polarization sensitivity of 2 μK arcmin (1:7 μK arcmin for the full array).

previous proposals COrE [6] and PRISM [7], a set of CMB polarization mission have been proposed in the USA (see e.g. [8], [9]). In Japan, the LiteBIRD proposal is currently in phase-A [10]. This re ects the awareness of the scienti c community that an unambiguous detection and characterizaiton of B-mode polarization from in ation cannot be achieved from ground-based measurements alone. There are two main problems: the need for a large sky coverage (the primordial B-mode signature in the Reionization peak is at the largest angular scales) and the need for a wide frequency coverage (to monitor overwhelming Galactic polarized foregrounds). Ground-based measurements su er in both cases. Atmospheric noise, following a Kolmogorov statistics, is severe at large angular scales, and anisotropic ground pickup may seriously contaminate the detected signal at these scales. Atmospheric transmission and stability rapidly become a serious limitation at frequencies higher than 250 GHz, even in the best observing sites on Earth. Coordinated ground-based e orts can do extremely well in the well-known 40, 90, 140 GHz atmospheric windows and at intermediate and small angular scales [11], but they have very serious limitations at higher frequencies (where the polarized dust foreground must be monitored) and at large angular scales.

The CORE instrument concept described in this paper has been conceived to minimize complexity and single-point criticalities, maximizing reliability in development, test, commissioning and operation. It uses a well developed, mirrors-only cross-Dragone telescope, with mirrors smaller than the mirrors used in Planck. It uses, as a baseline, simple single-frequency single-polarization detectors (dual-polarization is considered only for the lowest frequencies, as explained further on). It does not use a polarization modulator, avoiding critical cryogenic

mechanisms. Exploiting the good angular resolution provided by the telescope, it is possible to synthesize in the analysis perfectly circular observation beams, so that the polarization of the sky can be measured simply by rotating the entire instrument. With a smaller aperture, this would not be possible, and the added complexity of a polarization modulator would be required to separate real sky polarization and signal produced by the rotation of an elliptical beam. In addition, the angular resolution provided by the 1.2m re ector allows for internal delensing of the data, a real plus when looking for such a low level of B-mode polarization [12].

In Table 1 we anticipate the baseline con guration for the multi-band polarimeter, and its performance.

The rest of the paper is organized as follows: in the second section we describe the different telescope options which have been considered, taking into account the size constraints coming from the launcher, the need for su cient angular resolution, the need for a wide, high Strehl ratio, and possibly planar and telecentric focal plane. In the third section we discuss advantages and disadvantages of a mechanical polarization modulator, our baseline choice of avoiding its use, and our approach in case it is found to be required in the phase-A study. In the fourth section we describe the general design of the focal plane array and its optimization in terms of size, number of detectors, weight of the di erent bands. In the fth section we describe the selected detectors technology (Kinetic Inductance Detectors) and its implementation in the di erent frequency bands; the optical coupling and the readout electronics. In the sixth section we describe the cryogenic system. In the seventh section we describe the plan to calibrate the instrument. In section eight we describe a downscoped con guration of the instrument, with reduced aperture of the telescope (0.8m), reduced number of detectors (900), covering a reduced frequency range (100 to 600 GHz). We conclude comparing our baseline instrument to other proposals, in terms of gure of merit for the measurement of CMB B-modes.

2 Telescope

A combination of science requirements and practical constraints drive the choice of the telescope. The science requirements are (i) a focal surface with su ciently large di raction limited eld of view (DLFOV) to accommodate the 2100 detectors, (ii) entrance aperture size of 1.2 m to give a resolution between 7' and 8' at 145 GHz, and (iii) low instrumental polarization. Cost, the space mission implementation, and experience with previous mm-wave telescopes suggest a compact, low mass telescope, and re ectors that are su ciently small to be manufactured as a single segment of silicon carbide (silicon carbide has been space proven with the Herschel and Aladin missions). A quanti cation of the level of instrumental polarization tolerable with CORE is awaiting a more comprehensive study of systematic uncertainties.

The baseline detector technology for CORE also imposes constraints on the optical design. CORE will implement arrays of lens-coupled kinetic inductance detectors fabricated on at wafers. Therefore, the focal surface should be locally at and telecentric. The optical design needs to provide a focal surface that is either planar, or can be tiled with at detector wafers.

We investigated two designs: a two-mirror Gregorian, and a crossed-Dragone. Both designs have rich heritage with CMB experiments [13]. Most recently, WMAP and Planck used o -axis Gregorian telescopes. Tran et al. [14] showed that with equal aperture sizes a crossed-Dragone system can provide larger DLFOV compared to a Gregorian. (We follow

standard convention designating an area in the focal surface 'diffraction limited' when the Strehl ratio is larger than 0.8.)

2.1 Gregorian Design

2.1.1 All Reflective Design

The basic two-mirror Gregorian design has a parabolic primary and an ellipsoidal secondary. In Gregorian-Dragone designs, astigmatism or both astigmatism and coma are canceled to first order [13]. We began our analysis with a Gregorian-Dragone design in which astigmatism is canceled to first order [15] and used the optimization features available with a commercial ray tracing program[1] to increase the DLFOV over the frequency range between 60 and 600 GHz. Each of the reflector surfaces was described as a figure of revolution $z(r)$ by

$$z = \frac{cr^2}{1 + \sqrt{1 - (1+k)c^2r^2}} + \sum_{i=1}^{n} a_i r^{2i}; \qquad (2.1)$$

where k is the conic constant and c is the radius of curvature. Surfaces for which $a_i = 0$ for all i are conics of revolution. During the numerical optimization we let all the parameters in Equation 2.1 vary, as well as the parameters defining the relative orientations of the surfaces. The parameters of a system that gave a sufficiently large DLFOV are given in table 2. The system is shown in figure 1. We note that the focal surface is not flat. It is a shallow cone. We could not find a solution with a sufficiently large DLFOV and flat focal surface.

Figure 1 : 1:2 m Gregorian design and DLFOV contours for 60 GHz (black, outer), 90 GHz (blue), 130 GHz (red), 160 GHz (yellow), 220 GHz (magenta), 340 GHz (cyan), 450 GHz (green), and 600 GHz (black, inner).

This design has a 12 , 40 cm field of view at 60 GHz. The configuration is compact, and the system is conducive to strong baffling. The instrumental polarization across the entire

[1] CodeV by Synopsys Inc.

Primary mirror		Secondary mirror		Telescope geometry	
	136 cm 120 cm	97 cm 67 cm		D_m	120 cm
c	-5:94 10 ^{3}	0.0127		L_m	165 cm
k	-0.981	-0.319		L_s	148 cm
a_2	2:45 10 ^{9}	1:06 10 ^{9}		h	80:3 cm
a_3	3:67 10 ^{13}	-7:06 10 ^{13}			11:7
a_4	-3:35 10 ^{17}	1:20 10 ^{15}			3
a_5	1:40 10 ^{21}	-2:72 10 ^{19}		$_0$	51:2
a_6	-2:25 10 ^{26}	2:36 10 ^{23}			
Focal ratio, F		1.6 at center, increases by 7 % at focal plane edges			
160 GHz DLFOV		Az El = 7:6 7:8 , 85 F 73 F			
Focal Surface Location		Center	Az. edge	+ El. edge	El. edge
Instrumental polarization (%)		0.02	0.02	0.02	0.03
Polarization rotation ( )		0	6:4	0	0

Table 2 : Parameters for the CORE Gregorian design. Surface parameters refer to Equation 2.1; parameters determining the overall telescope geometry are de ned in Granet 2002 [16]. The parameters describing the focal plane dimensions are given at 160 GHz in degrees and in units of F (= 1 :875 mm) to facilitate comparison between di erent telescope con gurations. The variation in the focal ratio F across the focal surface gives a 160 GHz DLFOV that is larger in degrees in the elevation direction, but smaller in F .

focal plane, calculated at 145 GHz by assuming n; k = 1445; 1455 for aluminum [17], are below 0.05 %, but polarization rotation exceeds 6 at the azimuth edge of the focal surface. There is no polarization rotation along the symmetry plane of the system; see table 2. A signi cant drawback for this design is the non- at, non-telecentric focal surface. We concluded that if a Gregorian design is to be used, it requires additional image correction.

2.1.2 Re ective/Refractive Design

Figure 2 shows a Gregorian system with one additional alumina lens n(= 3 :1). Table 3 gives the parameter of the system. It has been optimized in a similar fashion to the one described in Section 2.1.1. The focal surface is at and nearly telecentric; the largest deviation from telecentricity is at the negative elevation edge (the lower part) of the FOV at a level of 4.1 degrees. This design provides 8:2 9:5 , 36 cm 36 cm, DLFOV at 60 GHz. These values are smaller than those for the all-re ective system. A more robust comparison that takes the focal ratios into account also shows that this system's performance falls short of the all-re ective one; see the lines giving the number of F at 160 GHz in tables 2 and 3. We could not t all 2100 of CORE's detectors in the focal plane.

The lens is 44 cm in diameter with an optical aperture diameter of 42 cm in diameter, and a mass of 6 kg. The system is compact and the aperture of the lens causes vignetting for elds near the edge of the focal plane, as can be seen in gure 2. Assuming tophat illumination of the primary, the throughput for this edge of the focal plane is reduced by 7 %. Vignetting reduces the throughput for the elds at both azimuth edges of the focal plane by 6 %.

The anti-re ection coating (ARC) of the lens presents a challenge. Broad, = = 160 % ARC are required with di erential re ection su ciently small to give low instrumental polarization. Although the development of broad-band ARC is an active area of research [18 20], the development of this bandwidth ARC on alumina has not been demonstrated, let

alone with low instrumental polarization. In table 3 we give expected levels of instrumental polarization assuming an uncoated alumina lenses. The levels are substantial but are likely over-estimates. The magnitude of polarization rotation in this system is similar to that in the all-re ective system.

In summary, the optical performance of the re ective/refractive system falls short of the requirements and the ARC presents a technical risk.

Figure 2 : 1:2 m Gregorian design with an alumina lens and DLFOV contours for 60 GHz (black, outer), 90 GHz (blue), 130 GHz (red), 160 GHz (yellow), 220 GHz (magenta), 340 GHz (cyan), 450 GHz (green), and 600 GHz (black, inner).

	Primary mirror	Secondary mirror	Alumina Lens		Telescope geometry
	150 cm 130 cm	100 cm 70 cm	44 cm	D_m	120 cm
c	-6:47 10 ^{3}	0.0154	-2:67 10 ^{3}	L_m	145 cm
k	-0.974	-0.333	0	L_s	140 cm
a_2	-1:02 10 ^{9}	6:08 10 ^{10}	1:76 10 ^{6}	h	76:3 cm
a_3	2:35 10 ^{14}	-1:91 10 ^{12}	-2:69 10 ^{8}		23:6
a_4	5:73 10 ^{19}	1:27 10 ^{16}	2:90 10 ^{11}		4
a_5	-3:50 10 ^{23}	5:34 10 ^{20}	4:64 10 ^{14}	$_0$	55:9
a_6	5:65 10 ^{28}	-1:35 10 ^{23}	-7:98 10 ^{17}		

Focal ratio, F	1.88 at centre, varies by 17 % across focal plane
160 GHz DLFOV	Az El = 6:4 7:2 , 68 F 75 F

Focal Surface Location	Center	Az. edge	+ El. edge	El. edge
Instrumental polarization (%)	0.26	2.7	3.6	1.8
Polarization rotation ( )	0	5:7	0	0

Table 3 : Same as table 2 but for the Gregorian design with an alumina lens.

2.2 Crossed Dragone

The crossed-Dragone con guration more naturally provides a at, telecentric focal plane and therefore it is a good match to focal planes with arrays of detectors that are micro-fabricated on at silicon wafers [14]. The con guration has heritage with the QUIET and ABS CMB polarization instruments [21, 22], and is currently the baseline for the JAXA-led LiteBIRD mission [23]. It is being considered for the CMB-S4 project [24].

For CORE we started with the 40 cm LiteBIRD telescope, scaled it up to 1:2 m aperture, and re-optimized in a process similar to that described in Section 2.1.1. The design included anamorphic surfaces, that is, surfaces with di erent radii of curvature in two orthogonal directions. The equation describing the surface $z(r)$ is

$$z = \frac{\frac{x^2}{R_x^2} + \frac{y^2}{R_y^2}}{1 + \sqrt{1 - (1 + k_x)\frac{x^2}{R_x^2} - (1 + k_y)\frac{y^2}{R_y^2}}} + A_{n;r}\left((1 - A_{n;p})x^2 + (1 + A_{n;p})y^2\right)^n; \qquad (2.2)$$

where R_x and R_y are the radii of curvature, k_x and k_y are the conic coe cients, and $A_{n;r}$, $A_{n;p}$ de ne the higher order deformation coe cients with $n = 2; 3; 4; 5$. When the higher order coe cients are zero this type of surface is called biconic. Figure 3 shows the system and Table 4 gives its parameters.

We found that with only two mirrors the system was too big to t within the satellite envelope. Therefore we added a at tertiary fold mirror to make the system more compact. This at mirror could be replaced by a re ective polarization modulator, if polarization modulation is deemed necessary. Figure 4 gives solid model views of the telescope integrated within the payload module and sunshields. The telescope was rotated about the boresight to put the focal plane close to the main satellite body, reducing the need for additional supports. This was also the only orientation in which the telescope was completely shadowed by the sun-shields.

The focal plane is at with a DLFOV greater than 12 degrees across at 160 GHz. It gives approximately 4 times the number of F units at 160 GHz compared to the all re ective Gregorian system, and a larger factor when compared to the partially refractive Gregorian. It is telecentric to within 3:5 over the entire FOV, and within 2 , which is 10 % of the beam divergence angle at the focal plane, at eld angles of less than 2:8 . Experience indicates that the system can be further optimized for even stronger telecentricity at the expense of DLFOV area at the edges of the focal plane that are currently not used. The instrumental polarization induced by the re ectors is a factor of 2-3 larger than the re ective Gregorian design, but still below 0.1%. There is signi cantly lower polarization rotation, a consequence of the atter re ecting surfaces.

An initial challenge with the crossed Dragone system was ba ing of the focal plane to reject stray light. To improve ba ing we embedded the portion of the DLFOV that is used for detectors inside a 'bucket', and a collar was added around the entrance aperture of the system; the bucket and collar are shown in grey gure 4. The default is all the paylod, including the collar, at 40 K.

With these additions there is no direct view from the focal plane to the sky. The focal plane area populated by detectors is bounded by the blue dash-dot line in Figure 3 and is smaller than the total available DLFOV.

We analyzed the crossed-Dragone design using physical optics to determine the far eld beam shape at 145 GHz for various positions on the focal plane. We assumed a Gaussian

Figure 3 : 1:2 m aperture CORE telescope and DLFOV at 160 GHz (yellow), 220 GHz (magenta), 340 GHz (cyan), 450 GHz (green), and 600 GHz (black). The DLFOV at lower frequencies is larger than that shown for 160 GHz The 50 cm diameter usable FOV (dash dot blue) is limited by ba es, not optical performance.

	Primary mirror	Secondary mirror	Telescope geometry	
	131 cm 152 cm	125 cm 146 cm	D_m	120 cm
R_x	-1:15 10^3	8:29 10^2	L_m	112 cm
R_y	-7:14 10^2	8:33 10^2	L_s	264 cm
k_x	2.97	-0.574	h	765 cm
k_y	-3.55	-7.31		13:8
$A_{2;r}$	3:02 10 ^{10}	1:31 10 ^{9}		90:2
$A_{3;r}$	9:54 10 ^{18}	3:05 10 ^{14}	$_0$	104
$A_{4;r}$	-1:63 10 ^{22}	-8:17 10 ^{19}		
$A_{5;r}$	-3:49 10 ^{34}	2:36 10 ^{24}		
$A_{2;p}$	-1:027	0:183		
$A_{3;p}$	-0:255	0:0671		
$A_{4;p}$	-0:281	0:259		
$A_{5;p}$	-0:914	0:669		

Tertiary mirror	104 cm 74 cm			
Focal ratio, F	2.54 at centre, varies by 5 % across focal plane			
160 GHz DLFOV	Az El = 14:0 12:9 , 159 F 140 F			
Focal Surface Location	Center	Az. edge	+ El. edge	El. edge
Instrumental polarization (%)	0.06	0.07, 0.05	0.07	0.05
Polarization rotation ( )	0	0:6	0	0

Table 4 : Parameters for the CORE Crossed Dragone design. Surface parameters refer to Equation 2.2; parameters determining the overall telescope geometry are de ned in Granet 2001 [25].

beam propagating from the focal plane outward. The Gaussian beam had a waist w_0 =

Figure 4 : Perspective views of the telescope and focal plane relative to the spacecraft's sunshields and bus. Only the edge of the entrance aperture of the enclosure is shown for clarity (gray).

$0.216\sqrt{T_e(\mathrm{dB})}F = 5.14$ mm with an edge taper of -20.5 dB on the primary mirror and $F = 2.54$. For this first round of analysis we did not include the baffling structures.

Figure 5 shows representative orthogonal cuts of the far-field beams at 3° off-axis along the x axis of the telescope (see figure 3). These field positions correspond to locations that are 15 cm from the center of the focal plane in the horizontal directions in the right panel of figure 3. We present results for only one polarization. The orthogonal polarization, which was also propagated to the sky, is co-located and the differential gain between the two polarizations is -41 dB over the main beam.

Figure 5 : Orthogonal co-pol and cross-pol cuts of the 145 GHz far field beams at off-axis angles of 3° along the x direction of the telescope, as indicated in figure 3.

We fit two-dimensional Gaussian to the far-field beam patterns to extract full-width at half-maxima (FWHM) from which we calculate beam ellipticities. Ellipticity is defined as $1 - b/a$, where a and b represent the larger and smaller FWHM, respectively. Cross-polarization levels are low, -48 dB at a maximum for the beams at 3°, but the co-polar components of the orthogonal polarizations show some aberration and have ellipticities of 6 and 8 % for the -3° and +3° directions, respectively. A summary of the characteristics of the beams at several field locations is given in table 5.

The physical optics study of the telescope performance for a variety of focal plane po-

sitions and frequencies is ongoing. There is also initial work currently underway to simulate the far sidelobes and examine the impact of the shielding on the optical performance.

Beam	FWHM (arcmin)	FWHM (arcmin)	$_0$	$_0$	Ellipticity
Y = 3 - X-Polarization	7.16	7.80	0.0001	0.0195	0.082
Y = 3 - Y-Polarization	7.16	7.80	0.0001	0.0195	0.082
Y = 3 - X-Polarization	7.24	7.73	0	-0.022	0.063
Y = 3 - Y-Polarization	7.24	7.73	0	-0.022	0.063
Y = 4 - X-Polarization	7.14	8.10	0.0002	0.0252	0.118
Y = 4 - Y-Polarization	7.14	8.10	0.0002	0.0252	0.118
Y = 4 - X-Polarization	7.26	7.92	0.0001	-0.0285	0.083
Y = 4 - Y-Polarization	7.26	7.92	0.0001	-0.0285	0.083

Table 5 : Far eld beam parameters for two orthogonal polarizations of Gaussian beam inputs located at o -axis angles of 3 and 4 along the x direction of the telescope (as illustrated in gure 3), at 145 GHz The coordinates $_0$ and $_0$ give the o sets of the beam centroids relative to a ray traced along the center of the input Gaussian.

2.3 Telescope Summary

WMAP and Planck used o -axis Gregorian telescopes. However, their useable DLFOV was smaller than that of CORE and their detector technology is no longer suitable for modern instruments that use thousands of focal plane elements. Such instruments require a large, at, and telecentric focal plane. The two mirror Gregorian falls short o the requirements. We attempted to populate this design with 10 cm edge-to-edge at tiles that were locally telecentric at the center of the tile. However, the optical performance at the edge of these tiles failed to be di raction limited.

The two-mirror Gregorian with the alumina lens gives an optical performance that is close to the requirements but the anti-re ection coating introduces a technology risk, and a spurious polarization risk. We selected the crossed-Dragone as the baseline because it gives a large, at, telecentric DLFOV, and it ts within the satellite envelope. A full analysis of the system is ongoing. Table 6 summarizes the advantages and disadvantages of the systems we analyzed.

	Gregorian	Crossed Dragone
Pros	Small re ectors No lens: high TRL Easy to ba e	Large, at, telecentric DLFOV Low instrumental and low polarization rotation
Cons	No lens : Smaller, non- at DLFOV With lens: low TRL; insu cient DLFOV	Larger re ectors Ba ing more challenging

Table 6 : Advantages (Pros) and disadvantages (Cons) of the optical systems considered for CORE.

3 Polarization Modulator

In CORE polarization modulation is achieved by means of an optimized telescope pointing strategy, leading to frequent scans of the same sky pixel with di erent orientations of the

Figure 5. The best- tting results of the velocity gradient for the ionized gas in the MUSE eld. During the tting process, we rotated the velocity map at a certain angle and calculated the ux-weighted average of the velocity in each column. The best- tting direction of the velocity gradient is determined to have the lowest rms in the corresponding residual velocity map (velocity map – velocity gradient). Such an analysis determined the best- tting direction of the velocity gradient, 7.1 deg clockwise from the west as shown in Fig. 3. The MUSE velocity map is then rotated accordingly to align the velocity gradient east-west here. Upper panel: the H ux weighted velocity as a function of the distance from the eastern edge of the MUSE eld, after the rotation. The black dots show the averaged velocities, weighted by the H ux from spaxels in each column. The red solid line shows the best- tting velocity gradient. Lower panels: the rotated velocity map and the corresponding residual map after removing the best- tting velocity gradient.

3.2.1 Kinematics of the H OC

From the integrated spectrum of the whole OC in the MUSE eld, the redshift is measured to be 0.0241. The OC is likely moving westward as suggested by the umbrella-like X-ray morphology and the SE H trail (Fig. 2; Yagi et al. 2017). The H velocity map in Fig. 3 shows a nearly east-west velocity gradient. We estimate the velocity gradient by minimizing the velocity residuals relative to a model with a constant gradient from the MUSE velocity map. An angle of 7.1± 1.0 deg clockwise from the west, as shown in Fig. 3, results in the minimal velocity residual. The velocity gradient along this direction is substantial, 12 km s^{-1} per kpc. The H OC has a total velocity gradient of 200 km s^{-1} nearly aligned east-west (Figs 3 and 5). Such a large velocity gradient is higher than those typically found in isolated H clouds (e.g. Cannon et al. 2015). We can also estimate the cloud's dynamical mass if we assume that the velocity gradient is due to rotation in a stripped disc. We extrapolate the velocity gradient (12 km s^{-1} per kpc) to the OC's radius of 30 kpc, then the dynamic mass $M = v^2 r/G = 9.0 \times 10^{11}$ M . Thus, if the observed velocity gradient of the OC is the imprint of the rotation in the disc of its parent, its parent must be a massive galaxy. On the

Downloaded from https://academic.oup.com/mnras/article/505/4/4702/6290511 by guest on 23 September 2021

Figure 7. The emission line ratios in nine large spatial regions of the A1367 OC. The dashed, solid, and dotted lines show the criteria (from Kewley et al. 2001, Kauffmann et al. 2003 and Cid Fernandes et al. 2010) to separate the regions of SF, composite (Comp), AGN, and LI(N)ER, respectively. Typical errors in the ratios are plotted on the data points with the largest [O II]/H ratio (from the region at RA 10 arcsec and Dec. 8 arcsec in Fig. 3). The solid orange lines show the fractions (from 0 to 1) of H ux from radiative shocks as predicted by the models in Rich, Kewley & Dopita (2011). While the first two plots may suggest these regions as H regions, the [O]/H ratios in these regions are too high and there is no evidence of SF from the GALEX data.

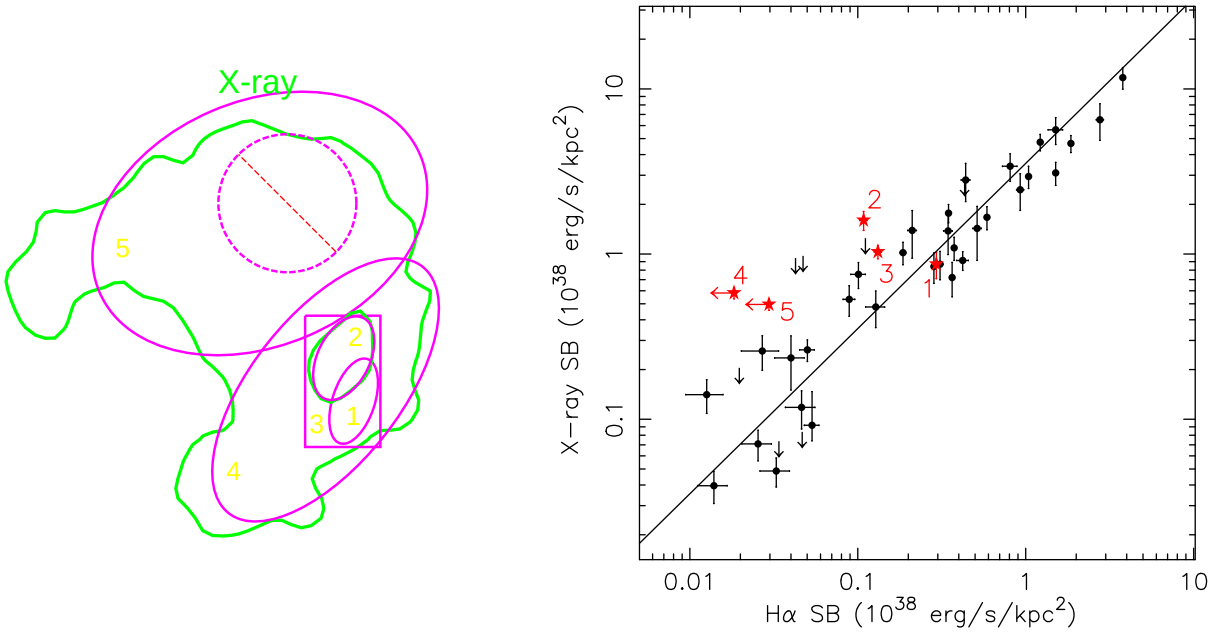

Figure 8. Left-hand panel: regions used to study the H X-ray correlation. Regions 1 and 2 are ellipses around the H and X-ray peaks, respectively. Region 3 is a box excluding regions 1 and 2. Region 4 is an ellipse excluding region 3. Region 5 is an ellipse excluding the bright X-ray source and region 4. For the H emission, galaxies, background sources, and H regions are all excluded. The same three-colour composite image as shown in Fig. 2 is shown here, with the X-ray contours in green. Right-hand panel: the measured H and X-ray surface brightnesses for these five regions in red are plotted with the best- tting linear relation and all data points in black from Sun et al. (2021). For the A1367 OC, while the correlation around the H cloud is consistent with those for stripped tails still attached to their parent galaxies, the X-ray-to-H ratios are typically higher, which should not be a surprise for the OC in a much more advanced stage of evolution than the stripped tails. Note that only generous upper limits on the H emission are put for regions 4 and 5.

4 DISCUSSION

4.1 Origin of the OC

First, we check if the X-ray OC is a background galaxy cluster. We examined the X-ray spectral properties of the OC assuming different z, exceeding 0.024. For each assumed z, the best- tting T_X and L_X are derived. If the OC is a background cluster, it should lie on the L_X–T_X relation for groups and clusters (e.g. Giles et al. 2016). This analysis constrains the redshift to the range $0.14 < z < 0.29$ for the X-ray OC (1 arcmin = 148–261 kpc at this z range). Late galaxies in clusters in this redshift range should have an r-band magnitude of 17.8–19.6 AB mag, well within the detection limit of SDSS. However, within 150 kpc of the X-ray peak (for z = 0.14–0.29), none of the SDSS